Proc. Natl. Acad. Sci. USA
Vol. 92, pp. 1965–1969, March 1995
Biophysics

Molecular electronics of a single photosystem I reaction center: Studies with scanning tunneling microscopy and spectroscopy

I. LEE, J. W. LEE, R. J. WARMACK, D. P. ALLISON, AND E. GREENBAUM†

Oak Ridge National Laboratory, P.O. Box 2008, Oak Ridge, TN 37831

Communicated by Hans Frauenfelder, Los Alamos National Laboratory, Los Alamos, NM, November 17, 1994 (received for review June 4, 1994)

ABSTRACT **Thylakoids and photosystem I (PSI) reaction centers were imaged by scanning tunneling microscopy. The thylakoids were isolated from spinach chloroplasts, and PSI reaction centers were extracted from thylakoid membranes. Because thylakoids are relatively thick nonconductors, they were sputter-coated with Pd/Au before imaging. PSI photosynthetic centers and chemically platinized PSI were investigated without sputter-coating. They were mounted on flat gold substrates that had been treated with mercaptoacetic acid to help bind the proteins. With tunneling spectroscopy, the PSI centers displayed a semiconductor-like response with a band gap of 1.8 eV. Lightly platinized (platinized for 1 hr) centers displayed diode-like conduction that resulted in dramatic contrast changes between images taken with opposite bias voltages. The electronic properties of this system were stable under long-term storage.**

The photosynthetic apparatus in green plants and algae is contained in a unique cellular organelle, the chloroplast. The chloroplast is enclosed by a double membrane and contains thylakoids, which consist of stacked membrane disks (grana) and unstacked membrane disks (stromal region). Although scanning tunneling microscopy (STM) images of disrupted chloroplasts have been reported (1, 2), functional characterization of single isolated reaction centers has not yet been achieved. Thylakoids play an important role in electron transport during photosynthesis. With STM and scanning tunneling spectroscopy (STS), it is possible to investigate their operational electrooptical properties.

Photosystem I (PSI) reaction centers are embedded in the thylakoid membrane. They drive the light-dependent transfer of electrons from plastocyanin (a copper-containing soluble protein located in the luminal space of chloroplast thylakoids) to ferredoxin (a [2Fe-2S]-containing soluble protein located in the chloroplast stroma). The PSI complex contains two high molecular mass subunits, the products of the *psaA* and *psaB* genes (the gene products for the chlorophyll *a* protein of PSI), and many low molecular mass subunits (3, 4). The PSI reaction center measured by electron microscopy is about 10 nm × 15 nm (5–7), or 7 nm × 12 nm after correction for attached detergent. Alekperov *et al.* (8) used STM to image photosynthetic reaction centers of purple bacteria and used the tip to transfer molecules or clusters of molecules from one area to another within the scanning range.

The attachment of platinum on the reducing side of PSI has a significant effect on the electrical properties of PSI. This can be observed by transformed photobiocatalytic properties and a sustained steady-state vectorial flow of current (9, 10). In this paper, we describe the use of tunneling spectroscopy to characterize the electrical nature of bare and platinized PSI. For semiconductors, tunneling spectroscopy has been used to characterize surface states and to measure surface-state band gaps (11, 12). We show that a band gap can be clearly seen in bare PSI, and platinized PSIs can act as either a diode or a metal, depending upon the degree of platinization.

EXPERIMENTAL PROCEDURES

Spinach chloroplasts were prepared according to the procedure of Reeves and Hall (13), in which the chloroplast envelope is ruptured, exposing the photosynthetic membranes to the external aqueous medium. A drop of the thylakoid suspension was then placed on freshly cleaved mica. After about 30 sec, the excess solution was removed by absorption with filter paper at the edge of the disk. The concentration of the thylakoid suspension was adjusted (diluted 1:10 to 1:100 with distilled water) so that isolated thylakoids and some aggregates on the mica disk could be seen by optical microscopy. The sample was then sputter-coated with 3 nm of Pd/Au metal and imaged by scanning electron microscopy in vacuum and STM in air.

The PSI reaction centers together with their antenna complexes containing about 40 chlorophylls per photoactive P700 (PSI-40) were isolated from the thylakoids by detergent (Triton X-100) solubilization and hydroxylapatite column purification (14). The identification of PSI in solution was confirmed by absorption spectroscopy (absorption maxima at 440 nm and 672 nm in agreement with ref. 15).

The PSIs were platinized by coprecipitation with colloidal platinum. Briefly, this was performed chemically by reduction of $[PtCl_6]^{2-}$ in the PSI elution by hydrogen flowing in the head space of a reaction vessel that contained the gently stirred reaction medium. The degree of metallization was controlled by the time of precipitation and the flow speed of hydrogen. Platinization was conducted at 20°C at neutral pH (before and after the platinization, the pH of the samples was monitored by a Beckman ϕ 72 pH meter). The details of the platinization processes will be published elsewhere. This metallization process causes no harm to photosynthetic activity of PSI (J.W.L., P. Laible, T. G. Owens, I.L., and E.G., unpublished work).

For PSI imaging, the flat gold substrates were prepared by evaporation of 120 nm of gold onto freshly cleaved mica heated to a temperature of 300–400°C (16). Gold surfaces were chemically modified by a 30-sec immersion in 10 mM mercaptoacetic acid, rinsed thoroughly in water, and air dried. This procedure is designed to terminate the surface with negatively charged end groups to attract and immobilize the PSI, as shown in Fig. 1. A similar method with positively charged end groups has been previously used to immobilize DNA for STM imaging (17). The treated surfaces were incubated for a few minutes with a drop of PSI-containing buffer solution, rinsed in distilled water, and air dried before STM imaging. For comparison, control samples were prepared identically, except that buffer solution without PSI was used in the incubation. Fluorescence spectroscopy and atomic force microscopy (AFM) were used to compare the amount of PSI adsorbed on

The publication costs of this article were defrayed in part by page charge payment. This article must therefore be hereby marked "*advertisement*" in accordance with 18 U.S.C. §1734 solely to indicate this fact.

Abbreviations: STM, scanning tunneling microscopy; STS, scanning tunneling spectroscopy; PSI, photosystem I.

†To whom reprint requests should be addressed.

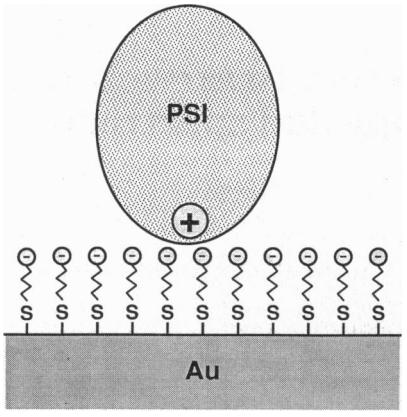

FIG. 1. Schematic illustration of the method used for electrostatic immobilization of PSI onto gold surfaces modified with mercaptoacetic acid.

untreated gold surface with surfaces treated with various surface-modifying reagents (i.e., 2-mercaptoethanol, 2-dimethylaminoethanethiol, thioacetic acid, mercaptoacetic acid, and mercaptoethane). The strongest adsorption of PSI was obtained on mercaptoethanol or mercaptoacetic acid-treated gold substrates. The systematic study detailing the immobilization of PSI on various chemically treated gold surfaces will be reported elsewhere (I.L., E. Wachter, J.W.L., D.P.A., E.G., and R.J.W., unpublished work).

STM images were recorded with a Nanoscope III (Digital Instruments, Santa Barbara, CA) in the constant-current mode, and spectroscopy was performed with a Nanoscope II. Mechanically cut Pt/Ir tips were used for both STM and STS studies. For the current–voltage (*I–V*) curves, the tip was held stationary while 400 data points, at a sample period of 400 μs per point, were taken by sweeping the sample potential between -1.0 V and 1.0 V. Each *I–V* datum represents an average of 4–40 scans. The absolute tip–sample distance is not known, but all data (with or without PSI) were taken at a distance where a -500-mV sample bias yielded a 160-pA tunneling current.

RESULTS AND DISCUSSION

Images. Preparations of disrupted choroplasts with intact thylakoids were imaged by optical microscopy, SEM, and STM. The latter two methods required thin Au/Pd metal coating to produce reliable images, since the thylakoids are large and nonconducting. The isolated thylakoids appeared as flattened spheres that ranged in size from 150 to 380 nm in diameter by 37–50 nm high. The fine details were obscured at the 6- to 10-nm scale due to the particle size of the metal coating.

PSI reaction centers were examined by STM without Pd/Au sputter coating, but with various degrees of platinization (none, light, and heavy) on treated gold substrates. Fig. 2 shows typical STM images of unplatinized PSI-coated substrates. The particles appeared uniform in size and consistently spread over the substrates, while the control samples (buffer on treated gold) exhibited no such structures. Also, no particles of like nature could be found on underivatized gold that had been incubated with the PSI solution. These observations are consistent with immobilization experiments which showed good adsorption only on gold surfaces with charged pendant groups (I.L., E. Wachter, J.W.L., D.P.A., E.G., and R.J.W., unpublished work). When the sample bias was reversed, no contrast variation was observed. Analysis of a number of images showed slightly elongated disk-like particles with dimensions 6 nm × 5 nm. For images taken by the same tip, the size uncertainty

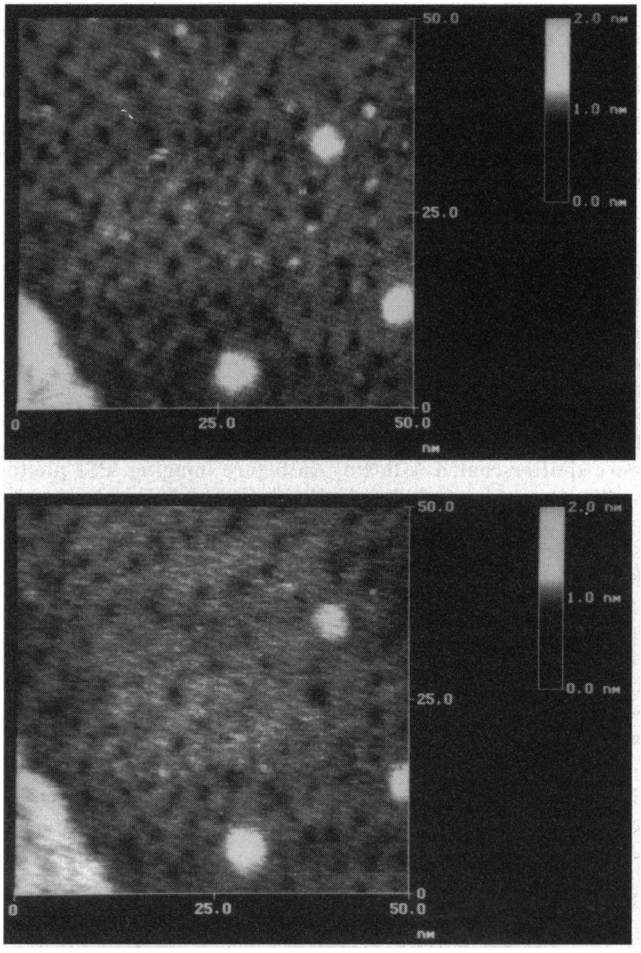

FIG. 2. STM images of bare PSI (i.e., without platinization) at bias voltages of 500 mV (*Upper*) and -500 mV (*Lower*). Note that there are no observable contrast changes between the images.

is ± 0.1 nm, but for those taken by different tips, the size uncertainty is ± 0.4 nm.

The average height of bare PSI reaction centers measured by STM is 0.4 nm, which is an order of magnitude lower than the estimated height of the PSI center. Height reductions have also been observed over various proteins (18, 19) and skeletal muscle glycogenolytic complexes (20). Negative heights were seen over tobacco mosaic virus (21, 22), purple membrane (23), and DNA (17, 24). These discrepancies in height have been attributed to the tip exerting increased pressure over poorly conducting adsorbates in attempting to keep the tunneling current constant. This results in lowered heights (contrast) over these adsorbates due to lack of mechanical stiffness in the scanning tunneling microscope. The exact conduction mechanism is not fully known (25), but the recorded heights are closer to those expected for very high gap resistances. Guckenberger *et al.* (22) used 10^{13}- to 10^{14}-ohm tunneling resistance over 18-nm-diameter virus particles to obtain a maximum 14-nm height in normally humid air. They explained that the condition of the tip (in particular, the slope of distance—voltage at constant current) and the humidity were controlling factors for their tunneling conditions. The gap resistance in our experiments was of the order of 10^9 ohms due to limitations in the electronics of the instrument used. Under these conditions the tip was very close to the surface, so that mechanical effects as well as changes in resistivity of the material in the gap are likely to alter the recorded heights of inhomogeneous surfaces. In any case, consistent images were readily obtained.

For lightly platinized (platinized for 1 hr) PSI reaction centers, similar topographic images were observed, but unexpectedly we found that the image contrast strongly depended on sample bias. In Fig. 3 *Upper*, the contrast of PSI completely disappears when the sample bias is positive (electrons tunneling from the tip to unoccupied sample states). In Fig. 3 *Lower*, the PSI reaction centers reappear as the sample bias changes to negative (electrons tunneling from the occupied sample states to the tip). Switching the bias back and forth several times always showed reversibility. This phenomenon was observed even after 4 months of storage with both the dry STM sample and a fresh sample prepared from the solution stored at 4°C. In the latter case, the PSI reaction centers did not completely disappear at positive bias, but a very strong contrast change was observed. Contrast changes at different bias voltages have also been observed on semiconductor surfaces such as silicon (26), aluminum on silicon (27), and gallium arsenide (28). For biological samples, this phenomenon was also observed by Golubok *et al.* (29) on photosynthetic bacterial membrane and by Luttrull *et al.* (30) on porphyrin-based molecules (molecules that mimic certain aspects of photosynthetic electron transfer).

Fig. 4 shows STM images of more heavily platinized (platinized for 4 hr) PSI reaction centers. In this case, the image contrast was unaffected by bias reversal at ±500 mV. The average apparent size of these PSI reaction centers is 9 nm × 7 nm by 0.5 nm in height. The horizontal dimensions are slightly larger than those measured on bare PSI reaction centers. Again, the apparent height is much less than that expected. This suggests that the heavily platinum-coated PSI does not form an electrically connected shell-like structure and that anomalous heights again result from the poorly conductive nature of PSI. Similar results were obtained on PSI that was platinized for 3 hr. However, some samples were prepared by using excessive metallization, for which heights more consistent with known dimensions were observed, indicating good electrical conductivity.

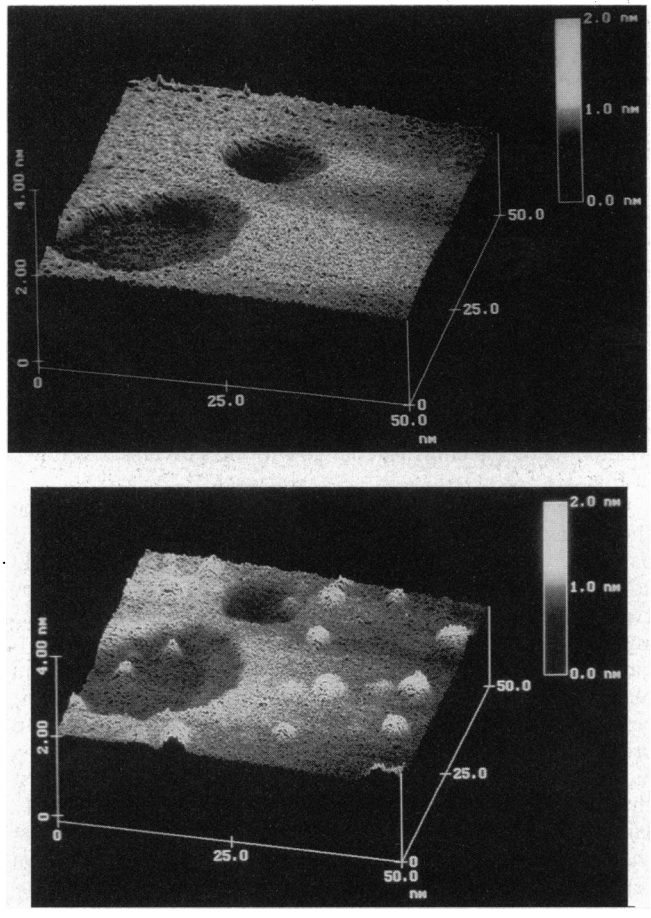

FIG. 3. STM images of lightly platinized (1 hr) PSI at bias voltages of 500 mV (*Upper*) and −500 mV (*Lower*). The strong contrast variations exemplified here were reversible with bias and could be switched back and forth repeatedly.

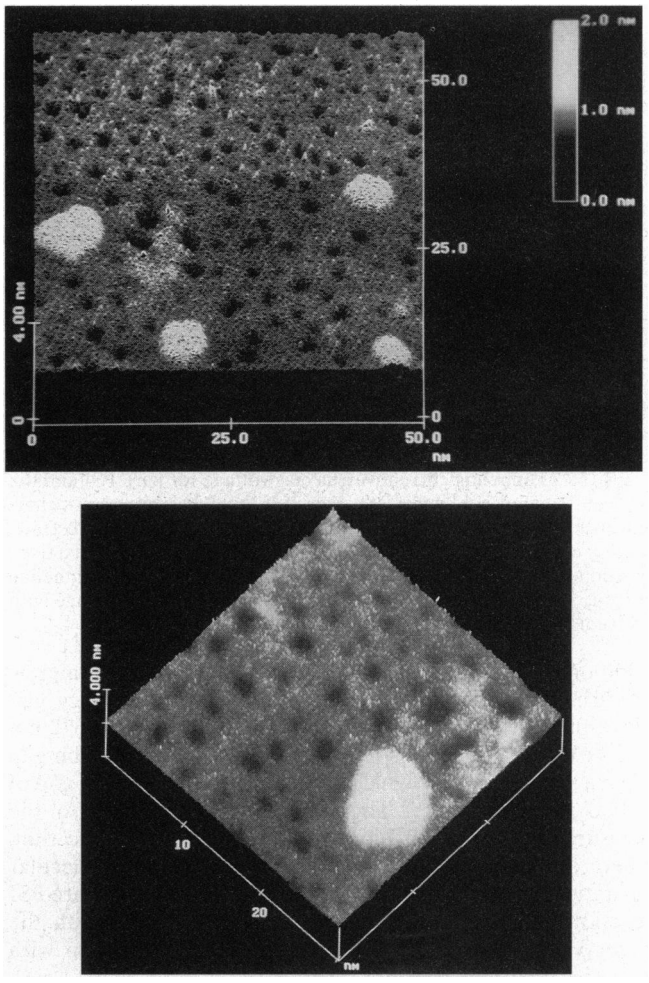

FIG. 4. STM images of PSI that had been platinum-pretreated for 4 hr before deposition. (*Upper*) Four PSI particles adsorbed on a gold surface. (*Lower*) Top-view image of PSI.

STS. To obtain additional information on the electrical properties of PSI and platinized PSI, we used tunneling spectroscopy with STM to obtain *I–V* curves at various positions on the samples. Fig. 5 shows *I–V* curves taken with the tip over bare PSI and over an adjacent area on the treated gold substrate. Over PSI the *I–V* curve shows the characteristics typical of a bandgap semiconductor [such as silicon (11) or gallium arsenide (31)], while over the treated gold substrate the *I–V* curve is characteristic of a typical metal (32).

It can be seen in Fig. 5 that the *apparent* conductance of PSI is much larger than of the substrate when the magnitude of the bias voltage is more than 500 mV. Higher apparent conductances over organic adsorbates have also been observed in other systems, such as DNA on gold (33) and protein on graphite (29). Again, this phenomenon is most likely due to electromechanical effects of the probe measurement. For inhomogeneous surfaces, the variation is introduced by moving from the substrate to the adsorbate at constant current.

The *I–V* plot for bare PSI can be numerically differentiated to give the relative density of states (34–38) (Fig. 6). It shows an energy gap of ≈1.8 eV from filled state to the first excited state. (An extended bias range over ±2 V did not reveal any

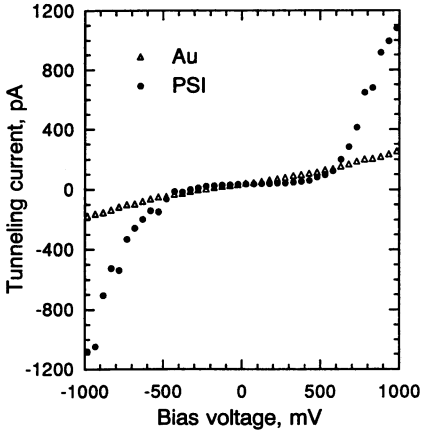

FIG. 5. Tunneling current versus bias voltage for bare PSI and the adjacent treated gold substrate. For PSI, the *I–V* curve shows characteristics typical of a semiconductor with bandgap. For the substrate, the *I–V* curve shows metallic characteristics. The tip was held at a fixed position so that −500 mV of bias voltage yielded 160 pA of tunneling current. Tunnel current is shown as a function of sample voltage with the tunnel tip at zero potential.

additional structures in the density of states but merely confirmed the structure shown in Fig. 6.) This energy gap corresponds to the strong optical absorption band at 672 nm (1.84 eV) for PSI from spinach (15). This is a transition gap from a single molecule which is different from the band gap of a bulk semiconductor. The result is more similar to the measurements done by Jeon *et al.* (39) on polyaniline film, where a transition gap of 4 eV corresponds to a molecular excitation of a π–π^* transition. Also, the *I–V* curve of bare PSI reaction centers is symmetric, which is consistent with the observed absence of contrast change in images taken with opposite polarities (see Fig. 2).

Fig. 7 shows *I–V* curves for lightly platinized PSI reaction centers compared with treated-gold substrates and bare platinum surfaces. Platinum responds similarly to gold but is shifted toward negative current with a slightly smaller slope. The heavily platinized PSI shows a metal-like *I–V* curve (not shown here) that closely follows that shown for platinum metal. Lightly platinized PSI shows a large asymmetry in the conductance between positive and negative biases. This is typical for doped semiconductors (40), in which tunneling current increases rapidly in forward bias (i.e., negative bias for *n*-type or positive bias for *p*-type) and remains small in reverse bias. In our case, similar to the *n*-type semiconductor, the platinum

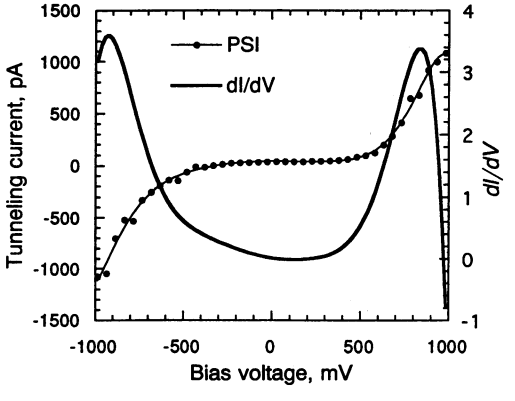

FIG. 6. *I–V* curve of bare PSI from Fig. 5 compared with the differential conductance, dI/dV, versus bias voltage from the same PSI data. The differential conductance reveals a bandgap of ≈1.8 eV. The line through the PSI points is a polynomial fit to the data.

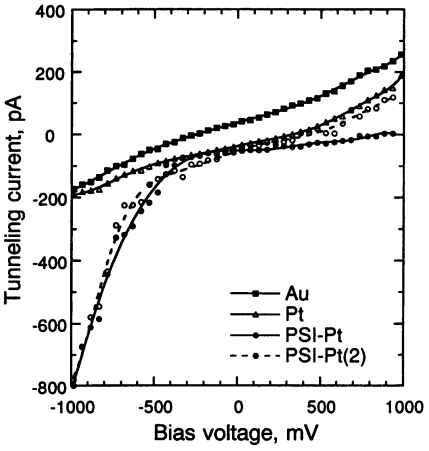

FIG. 7. *I–V* curves for treated gold, bare platinum, and lightly platinized PSI. PSI-Pt was taken on the sample shown in Fig. 3. PSI-Pt(2) is a sample of the same PSI-Pt solution but refrigerated for 4 months and then applied to a treated gold substrate. The *I–V* curves for gold and platinum show typical metallic characteristics. The diode-like *I–V* curves for platinized PSI show characteristics of an n-type semiconductor.

appears to fill the unoccupied states that are sampled at positive bias, resulting in a reduction of the relative tunneling current. This explains the changing contrast of the STM image that was observed at opposite biases. Thus, platinum appears to strongly interact with PSI and alter its electrical properties. The result is consistent with previous demonstrations that electrical contact with the reducing end of PSI can be achieved by precipitating colloidal platinum (J.W.L., P. Laible, I.L., T. G. Owens, and E.G., unpublished work), and the presence of the platinum greatly affects the photocurrent and photoconductivity of the metal–biological composite material (9, 10, 41).

The characteristics of the platinized PSI remained stable over a period of 4 months. The dry mounted sample (identified as PSI-Pt in Fig. 7) showed identical *I–V* curves after this period of storage in a desiccator. The solution from which this sample was prepared was stored at 4°C for 4 months and applied to a fresh substrate. The *I–V* curve for this aged sample (identified as PSI-Pt(2) in Fig. 7) still shows an asymmetry but not quite as strongly as the dry-stored sample. Either the degree of platinization was increased (42) or the PSI was slightly degraded in wet storage. This was also observed as a weakening of the contrast change with bias reversal as shown in Fig. 3.

Conclusions. PSI reaction centers obtained from spinach chloroplasts have been studied by STM and STS. The PSI particles were applied to treated gold surfaces for good adsorption and resistance to rinsing. They were identified by evaluating control experiments, by fluorescent tracing, by size and shape, by the progression of plantinization, and by evaluating their *I–V* response. The PSI reaction center had an observed size of 6 nm × 5 nm, and the heavily platinized PSI center had a size of 9 nm × 7 nm. The apparent heights are an order of magnitude less than expected, as is typical in many biological samples measured by STM. A strong contrast change for lightly platinized PSI was observed with opposite sample bias. Conversely, there was no apparent contrast change on either bare PSI or heavily platinized PSI reaction centers. These contrast changes are reflected in STS measurements.

By using tunneling spectroscopy, we have shown that various materials and degrees of platinization on PSI can be distinguished. Bare PSI reaction center shows the characteristics of a bandgap semiconductor or insulator, lightly platinized PSI

shows the characteristics of an n-type semiconductor, and heavily platinized PSI shows the *I–V* characteristics of platinum metal. We conclude that the interaction of platinum with PSI, and perhaps the properties of the platinum particles themselves, may be operative. Further investigation is warranted to clarify the causes of these interesting properties.

This research was supported by the U.S. Department of Energy. Oak Ridge National Laboratory is managed by Martin Marietta Energy Systems, Inc., for the U.S. Department of Energy under Contract DE-AC05-84OR21400.

1. Mainsbridge, B. & Thundat, T. (1991) *J. Vac. Sci. Technol.* **B 9,** 1259–1262.
2. Dahn, D. C., Cake, K. & Hale, L. R. (1992) *Ultramicroscopy* **42–44,** 1222–1226.
3. Fish, L. E., Kuck, U. & Bogorad, L. (1985) *J. Biol. Chem.* **260,** 1413–1421.
4. Fish, L. E. & Bogorad, L. (1986) *J. Biol. Chem.* **261,** 8134–8139.
5. Ford, R. C. & Holzenburg, A. (1988) *EMBO J.* **7,** 2287–2293.
6. Rögner, M., Mühlenhoff, U., Boekema, E. J. & Witt, H. T. (1990) *Biochim. Biophys. Acta* **1015,** 415–424.
7. Boekema, E. J., Wynn, R. M. & Malkin, R. (1990) *Biochim. Biophys. Acta* **1017,** 49–56.
8. Alekperov, S. D., Vasiljev, S. I., Kononenko, A. A., Lukashev, E. P., Panov, V. I. & Semenov, A. E. (1989) *Chem. Phys. Lett.* **164,** 151–154.
9. Greenbaum, E. (1985) *Science* **230,** 1373–1375.
10. Greenbaum, E. (1990) *J. Phys. Chem.* **94,** 6151–6153.
11. Feenstra, R. M., Stroscio, J. A. & Fein, A. P. (1987) *Surf. Sci.* **181,** 295–306.
12. Tromp, R. M. (1989) *J. Phys. Condens. Matter* **1,** 10211–10228.
13. Reeves, S. G. & Hall, D. O. (1980) *Methods Enzymol.* **69,** 85–94.
14. Lee, J. W. (1993) Ph.D. Dissertation (Cornell University, Ithaca, NY).
15. Mukerji, I. & Sauer, K. (1993) *Biochim. Biophys. Acta* **1142,** 311–320.
16. DeRose, J. A., Thundat, T., Nagahara, L. A. & Lindsay, S. M. (1991) *Surf. Sci.* **256,** 102–108.
17. Allison, D. P., Bottomley, L. A., Thundat, T., Brown, G. M., Woychik, R. P., Schrick, J. J., Jacobson, K. B. & Warmack, R. J. (1992) *Proc. Natl. Acad. Sci. USA* **89,** 10129–10133.
18. Miles, M. J., Carr, H. J., McMaster, T. C., I'Anson, K. J., Belton, P. S., Morris, V. J., Field, J. M., Shewry, P. R. & Tatham, A. S. (1991) *Proc. Natl. Acad. Sci. USA* **88,** 68–71.
19. Arakawa, H., Umemura, K. & Ikai, A. (1992) *Nature (London)* **358,** 171–173.
20. Edstron, R. D., Miller, M. A., Elings, V. B., Yang, X., Yang, R., Lee, G. & Evans, D. F. (1991) *J. Vac. Sci. Technol. B* **9,** 1248–1252.
21. Mantovani, J. G., Allison, D. P., Warmack, R. J., Ferrell, T. L., Ford, J. R., Manos, R. E., Thompson, J. R., Reddick, B. B. & Jacobson, K. B. (1990) *J. Microsc.* **158,** 109–116.
22. Guckenberger, R., Arce, F. T., Hillebrand, A. & Hartmann, T. (1994) *J. Vac. Sci. Technol. B* **12,** 1508–1511.
23. Guckenberger, R., Hacker, B., Hartmann, T., Scheybani, T., Wang, Z., Wiegräbe, W. & Baumeister, W. (1991) *J. Vac. Sci. Technol. B* **9,** 1227–1230.
24. Allison, D. P., Thundat, T., Jacobson, K. B., Bottomley, L. A. & Warmack, R. J. (1993) *J. Vac. Sci. Technol. A* **11,** 816–819.
25. Lindsay, S. M., Sankey, O. F., Li, Y., Herbst, C. & Rupprecht, A. (1990) *J. Phys. Chem.* **94,** 4655–4660.
26. Tromp, R. M., Hamers, R. J. & Demuth, J. E. (1986) *Phys. Rev. B* **34,** 1388–1391.
27. Hamers, R. J. & Demuth, J. E. (1988) *Phys. Rev. Lett.* **60,** 2527–2530.
28. Feenstra, R. M., Stroscio, J. A., Tersoff, J. & Fein, A. P. (1987) *Phys. Rev. Lett.* **58,** 1192–1195.
29. Golubok, A. O., Vinogradova, S. A., Tipisev, S. Y., Borisov, A. Y., Taisova, A. S. & Kolomytkin, O. V. (1992) *Ultramicroscopy* **42–44,** 1228–1235.
30. Luttrull, D. K., Graham, J., DeRose, J. A., Gust, D., Moore, T. A. & Lindsay, S. M. (1992) *Langmuir* **8,** 765–768.
31. Salemink, H. & Albrektsen, O. (1991) *J. Vac. Sci. Technol. B* **9,** 779–782.
32. Kuk, Y. & Silverman, P. J. (1990) *J. Vac. Sci. Technol. A* **8,** 289–292.
33. Lindsay, S. M., Li, Y., Pan, J., Thundat, T., Nagahara, L. A., Oden, P., DeRose, J. A., Kipping, U. & White, J. W. (1991) *J. Vac. Sci. Technol. B* **9,** 1096–1101.
34. Tersoff, J. & Hamann, D. R. (1983) *Phys. Rev. Lett.* **50,** 1998–2001.
35. Tersoff, J. & Hamann, D. R. (1985) *Phys. Rev. B* **31,** 805–813.
36. Baratoff, A. (1984) *Physica B* **127,** 143–148.
37. Selloni, A., Carnevali, P., Tosatti, E. & Chen, C. D. (1985) *Phys. Rev. B* **31,** 2602–2605.
38. Lang, N. D. (1986) *Phys. Rev. B* **34,** 5947–5950.
39. Jeon, D., Kim, J., Gallagher, M. C., Willis, R. F. & Kim, Y. T. (1991) *J. Vac. Sci. Technol. B* **9,** 1154–1158.
40. Kaiser, W. J., Bell, L. D., Hecht, M. H. & Grunthaner, F. J. (1988) *J. Vac. Sci. Technol. A* **6,** 519–523.
41. Green, E. (1989) *Bioelectrochem. Bioenerg.* **21,** 171–177.
42. Chiu, Y., Reed, M. L. & Schlesinger, T. E. (1992) *Appl. Phys. Lett.* **60,** 1715–1716.